SCIENCE CHINA
Information Sciences

• RESEARCH PAPER •

January 2025, Vol. 68, Iss. 1, 112401:1–112401:9
https://doi.org/10.1007/s11432-024-4093-1

MoS_2 synaptic transistor with one-step manufacture

Yihao GUO[1,2], Yang WANG[3], Wenjie DENG[1,2*], Yi WU[2], Jingtao LI[2], Kexin LI[1], Yuehui ZHAO[1], Songlin YU[3], Xiaoting WANG[1,2*], Yongzhe ZHANG[1,2*] & Hui YAN[2]

[1]*Key Laboratory of Optoelectronics Technology of Education Ministry of China, Faculty of Information Technology, Beijing University of Technology, Beijing 100124, China;*
[2]*Key Laboratory of Advanced Functional Materials, Ministry of Education, Faculty of Materials and Manufacturing, Beijing University of Technology, Beijing 100124, China;*
[3]*The 11th Research Institute of Electronics Technology Group Corporation, Beijing 100015, China*

Received 9 April 2024/Revised 28 April 2024/Accepted 8 July 2024/Published online 13 December 2024

Abstract The synaptic transistor, which is a neuromorphic device with brain-like functions, has garnered significant attention due to characteristics such as low energy consumption, high integration, multiple functions, and high computational efficiency. However, the current synaptic transistor possesses a complicated structure and involves complex manufacturing steps, which is not conducive to low-cost, large-scale bionic integration. Herein, we introduce a simple MoS_2 synaptic transistor exhibiting robust synaptic plasticity. This transistor utilizes magnetron sputtering manufacture to combine the process of device metal electrode deposition and the introduction of defect states, which helps streamline the manufacturing process into a single step. The long-term potentiation and long-term depression in photoelectric coordination are initially revealed. Subsequently, biological functions, such as double pulse facilitation and the transformation behavior of short-term memory to long-term memory, are thoroughly evaluated, along with learning-forgetting-relearning processes. Interestingly, the device exhibits robust synaptic plasticity until incident light angles down to 30° to imitate the multi-to-one axon-cellular synapses. Finally, a classical simulation of Pavlov's dog conditioned reflex is demonstrated along with the multiview extraction applications. The experimental results demonstrate a promising synaptic transistor with a simple structure, manufacturing technique, and excellent performance. This further indicates the potential for large-scale integration of bionic neuromorphic systems.

Keywords process optimization, artificial synaptic device, one-step manufacture, synaptic plasticity, bionic simulation

Citation Guo Y H, Wang Y, Deng W J, et al. MoS_2 synaptic transistor with one-step manufacture. Sci China Inf Sci, 2025, 68(1): 112401, https://doi.org/10.1007/s11432-024-4093-1

1 Introduction

With the advent of technological innovations such as artificial intelligence, big data, and 5G networks, applications such as image and video processing have been largely simplified. Image and video processing is a data-intensive application that involves significant data storage, transmission, computation, and management requirements. However, the current computing field is largely dominated by the traditional von Neumann architecture. This architecture separates the memory unit from the processing unit, which results in issues such as the memory wall, heat wall, and the end of Moore's law [1–3]. To address the escalating demands for data computation, there is a growing interest in exploring new computing architectures. Brain-like computing is an effective approach to overcome the bottleneck of the von Neumann architecture. In the nervous system of the human brain, the neurons and synapses, which are the fundamental units of information integration, form neural computing networks that enable effective information transmission, exchange, and processing [4–6]. Similarly, the concept of optical synapses was reported to enable simultaneous optical detection and synaptic functions by mimicking the operation mode of the human retina to achieve highly efficient computing [7–13]. The artificial synaptic devices can deliver low energy consumption, high integration, and efficient image processing capabilities suitable for information perception, storage, and computation.

Artificial synaptic devices based on dual-terminal memory storage have garnered significant academic interest due to characteristics such as simple structure and low energy consumption. However, the programming terminals of such double-ended artificial synaptic devices are shared with the reading terminals,

* Corresponding author (email: wjdeng@bjut.edu.cn, wxt22@bjut.edu.cn, yzzhang@bjut.edu.cn)

which may lead to weight destruction during data readout [14–17]. In contrast, three-terminal devices can achieve lossless weight updates given that in these devices, the programming is separated from the read terminal, and it usually operates as a field effect transistor (FET) device. The weight update of these devices depends on the regulation of various charge storage mechanisms, such as floating gate, ion regulation, and defect storage [17–24]. In terms of manufacturing technology, the realization of the current reported synaptic transistors is primarily based on the foundational configuration of the FET for secondary design. These methods involve inserting the floating gate layer, electrolyte layer, and the channel material surface treatment [17–24]. A simple structure of the synaptic transistor may also be realized by using ferroelectric material as the channel material [25, 26]. However, the synthesis of ferroelectric materials requires more precise stoichiometric ratios, temperature, atmosphere and pressure conditions. Ferroelectric materials possess specific phase transition properties, and they involve complex crystal structures and electrical bipolarities, which make it difficult to produce high-quality, large-size samples [27]. Further, this results in a relatively complex structure and cumbersome manufacturing steps, making them nonconducive to low-cost, large-scale bionic integration. This facilitates the need to design a synaptic transistor with a simple structure that can be easily realized to achieve large-scale bionic integration.

The practical feasibility of achieving synaptic plasticity by introducing defects to charge storage through channel material processing has been experimentally verified by several researchers [20, 21]. In addition, the bombardment of high-energy particles may easily cause defects in two-dimensional (2D) materials, which has been reported in previous studies [28–31]. In this work, we propose a one-step manufacture of MoS_2 synaptic FET, wherein the high-energy metal particles by magnetron sputtering are employed to simultaneously achieve a goal of metal electrode deposition and introduction of defects states. This helps realize a simple MoS_2 transistor with excellent synaptic plasticity. Then, we compare the synaptic plasticity of the device by magnetron sputtering with interface defects and the device by metal transferring without interface defects. It is found that only the former exhibits synaptic plasticity and corresponds to long-term potentiation (LTP) and long-term depression (LTD) under photoelectric coordination. Biological simulations involving excitatory postsynaptic current, spike-rating dependent plasticity (SRDP), and paired-pulse facilitation (PPF) for the proposed device are explored thoroughly next, demonstrating its ability to realize the basic synaptic features. In addition, robust synaptic plasticity until incident light angles down to 30° is achieved, which helps imitate the multi-to-one axon-cellular synapse. Finally, we simulate two applications that can be realized using this one-step manufactured MoS_2 synaptic FET, including Pavlov's dog conditioned response and multi-view extraction functions based on a 3×3 array. The feature graph "X" from images affected by noise is successfully extracted.

2 Results and discussion

The interfacial contact between metal and MoS_2 heavily depends on the metal preparation method [28–31]. When magnetron sputtering is used to deposit metal electrodes, metal atoms or clusters with high kinetic energy collide with the molybdenum disulfide lattice at high speed during the deposition process, easily forming covalent bonds with molybdenum disulfide or generating defects (Figure 1(a)) [28]. In contrast, when electrodes are prepared using metal transfer, the resulting metal/MoS_2 interface is connected by van der Waals forces without strong hybridization (Figure 1(b)) [28, 30]. Both methods are employed to manufacture MoS_2 FETs to verify our hypothesis, with the specific preparation process shown in Figure S1. Process (1) represents metal transfer, while process (2) depicts magnetron sputtering. The thickness of the exfoliated two-dimensional material is thin and in good contact with the metal electrode, as shown in Figure S2. The thickness of the MoS_2 channel is about 6 nm for each device, indicating that about five layers are mechanically exfoliated in the experiment (Figure S3). We tested the basic photoelectric performance of the two devices, with results shown in Figure S4. When the same laser power is used, the photocurrent increases as the incident light wavelength decreases. To assess potential neuromorphic performance, we conducted an adjustment test of synaptic weights by irradiating the two devices separately with paired pulsed lasers and recording the time-dependent current changes (Figures 1(c) and (d)). It was observed that the MoS_2 FET fabricated with magnetron sputtering electrodes maintains synaptic plasticity under the influence of light, whereas the device fabricated with metal transfer does not exhibit this effect. Furthermore, excitatory post-synaptic current (EPSC) tests of the two devices also support these findings (Figure S5). To verify the reproducibility of the method,

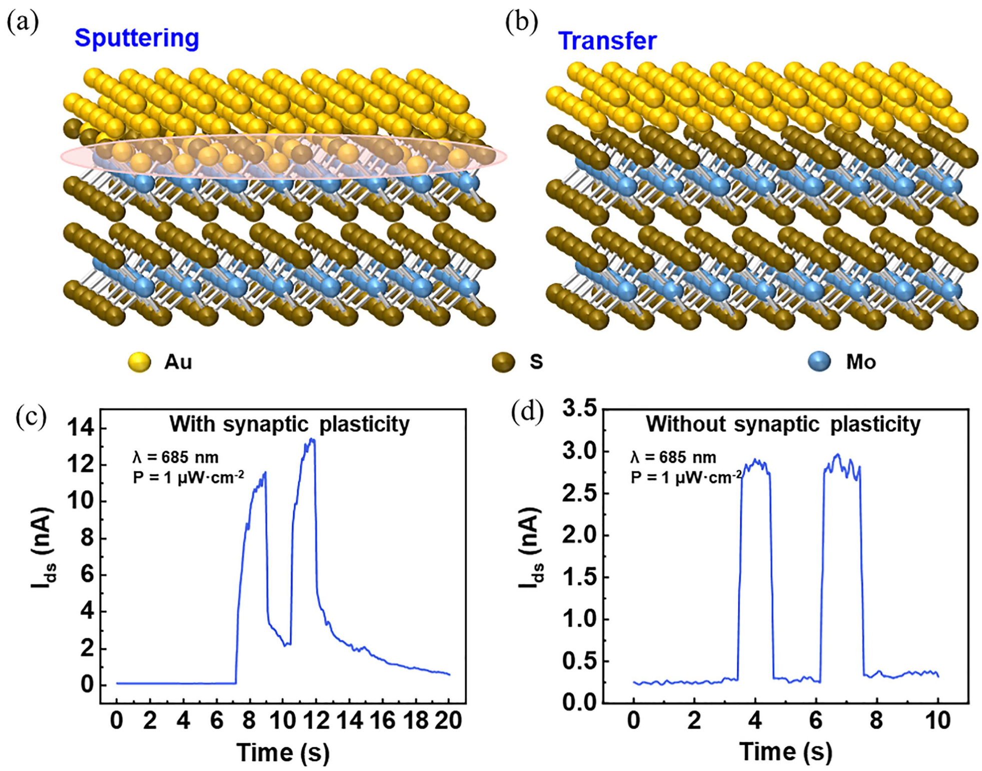

Figure 1 (Color online) Comparison of MoS_2 transistors prepared by different methods. (a), (b) Schematic diagram of interface contact at atoms level between metal and MoS_2 under different preparation methods. The pink circle highlight the damaged interface by sputtering metal. (c), (d) The optical pulse excited photo response for the two kinds of devices to observe the time-dependent trend of current. (a), (c) is corresponding to the magnetron sputtering and (b), (d) is corresponding to the metal transferring.

more devices were manufactured using both methods. The synaptic weight regulation and EPSC tests were consistently reproduced (Figure S6). These results initially indicate that MoS_2 FETs prepared with magnetron sputtered metal electrodes indeed possess synaptic plasticity.

The different method for manufacture leads to contract performances in the synaptic weight regulation test in Figure 1. In order to illustrate the synaptic plasticity mechanism in the sputtering device, we perform the Raman spectroscopy for the MoS_2. The fresh fabricated MoS_2 and metal deposited one are characterized respectively. Usually, MoS_2 with nearly no defects exhibits a Raman response dominated by two vibration modes: the in-plane E^1_{2g} vibration and the out-of-plane A_{1g} vibration at 532 nm [32–35]. When defects are present, a completely new vibration mode with unique characteristics is induced in the Raman spectrum which will broaden the width of the characteristic peak and raise a new peak [36–38]. The Raman spectra of MoS_2 before and after magnetron sputtering are shown in Figure 2(a). Two typical characteristic peaks, E^1_{2g} and A_{1g}, are clearly observed at 384.25 and 408.48 cm^{-1}, respectively. Following magnetron sputtering treatment, the width of the two characteristic peaks increased, and a shoulder appeared on the low-frequency side of peak E^1_{2g}. Sub-peak fitting treatment at peak E^1_{2g} revealed a new characteristic peak at 381.24 cm^{-1} (Figure 2(b)), suggesting the presence of defects induced by the sputtering process. The Raman spectra of MoS_2 before and after metal transferring are shown in Figure 2(c). Peaks E^1_{2g} and A_{1g} are located at 383.96 and 408.08 cm^{-1}, respectively. No new characteristic peaks or broadened peak widths were observed in the Raman spectra between the two spectra, indicating the absence of significant defects. These results imply that the synaptic plasticity of MoS_2 transistors prepared by magnetron sputtering is attributed to defects caused by high-energy particles bombardment during the metal deposition process. Therefore, we have successfully realized the two steps including the process of metal electrode deposition and defects states' introduction to achieve synaptic plasticity combining as one step, and then to achieve the simplify manufacture of the FET synaptic devices.

To gain a better understanding of the underlying mechanism behind the variation in channel current of the two types of MoS_2 transistors after illumination, we propose a physical model based on band theory to elucidate this phenomenon. The device based on magnetron sputtering is depicted in Figure 2(d).

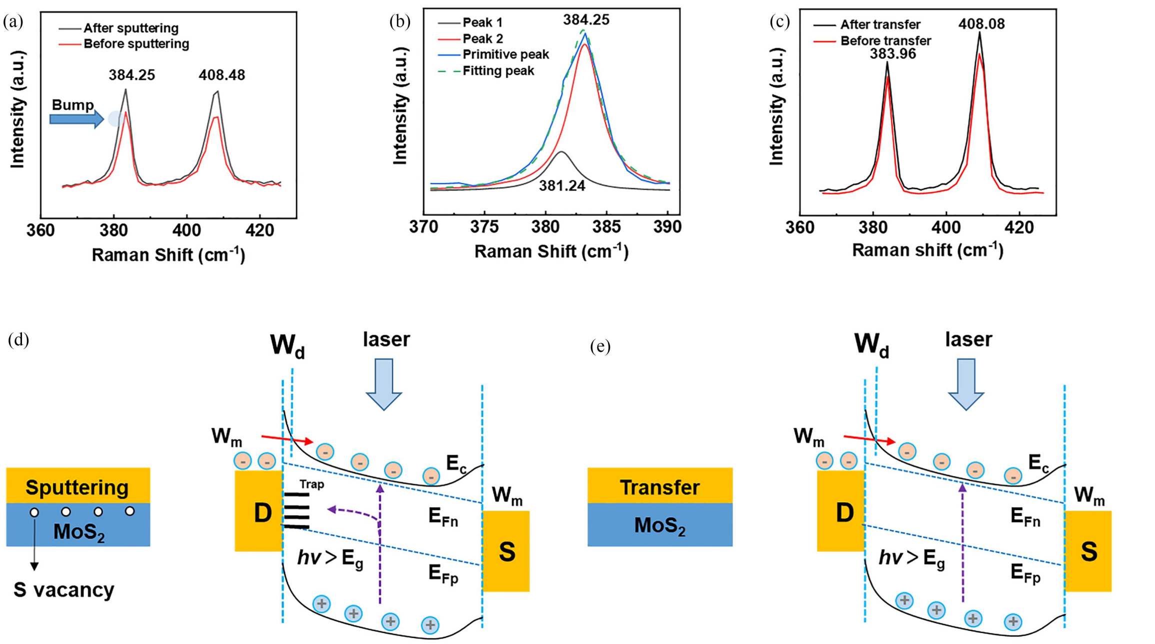

Figure 2 (Color online) Mechanism of the synaptic plasticity. (a) Raman spectrum of MoS_2 before and after magnetron sputtering. (b) Peak fitting of the Raman spectrum in (a). (c) Raman spectra of MoS_2 before and after metal transferring. Description of the synaptic plasticity mechanism through the charge capture and release process by (d) magnetron sputtering and (e) metal transfer technique.

A large number of photo-generated charge carriers are generated in the channel when MoS_2 exposed to light, electrons can be excited by photons to the conduction band, leaving holes in the valence band. The concentration of electrons in the conduction band increases, and the carriers move between the source-drain electrodes under the biased electric field. Due to the bombardment of magnetron sputtering high-energy particles, there are a large number of S-vacancy defects at the interface between electrodes and materials [28, 39, 40]. When the electrons move here, some of them are captured by the defect level and are gradually released to participate in conducting electricity [41–44]. Therefore, the current increases slowly during light illumination, and the conductance of the device will increase as the defect level is filled (Figure 1(c)). When the light is turned off, the trapped electrons by the defect are gradually released and combined with the hole, resulting in a gradual decrease in the device conductance and therefore a slow decrease in current. The photocurrent obtained by the second illumination will be larger than that obtained by the first illumination. This is because there are still some electrons produced by the previous light pulse stimulation and trapped by the defect level, these electrons are slowly released and then moved in the electric field until the lifetime is exhausted. These electrons have a superposition effect with the carriers produced by the second illumination, resulting in an increased electron concentration and thus a higher electric potential. After the light is turn off again, the reduction of conductance is a slow process similar to the former period, so the device has a memory function and can achieve synaptic bionics function. While a device based on the metal transferring exhibits a rapid increase in its current upon exposure to light (Figure 2(e)). Since there are no trap levels in the MoS_2 channel for charge storage, the carriers rapidly recombine after illumination, resulting in lower electron concentration and thus lower device conductance. This leads to a sharp decrease in the channel current, and the carrier superposition effect under multiple pulses cannot be realized (Figure 1(d)). And electrons are not disturbed by defects as they move, so conductance levels cannot be remembered.

To further explore the application potential of the MoS_2 synaptic transistor manufactured by the one-step method, we conducted bionic simulation tests of its synaptic characteristics. In the human nervous system, synaptic plasticity is a fundamental function for the brain learning and memory activities, allowing for the adjustment of synaptic weights through external stimuli [45]. The adjustment of synaptic weights is an indispensable feature to realize the function of artificial synapses. The proposed MoS_2 synaptic transistor is a three-terminal device, and its postsynaptic current (PSC) behavior can be adjusted by the gate voltage. Therefore, the device can realize the process of optical writing and electric erasure. As shown in Figure 3(a), the synaptic weight gradually increases after 12 consecutive optical pulses are

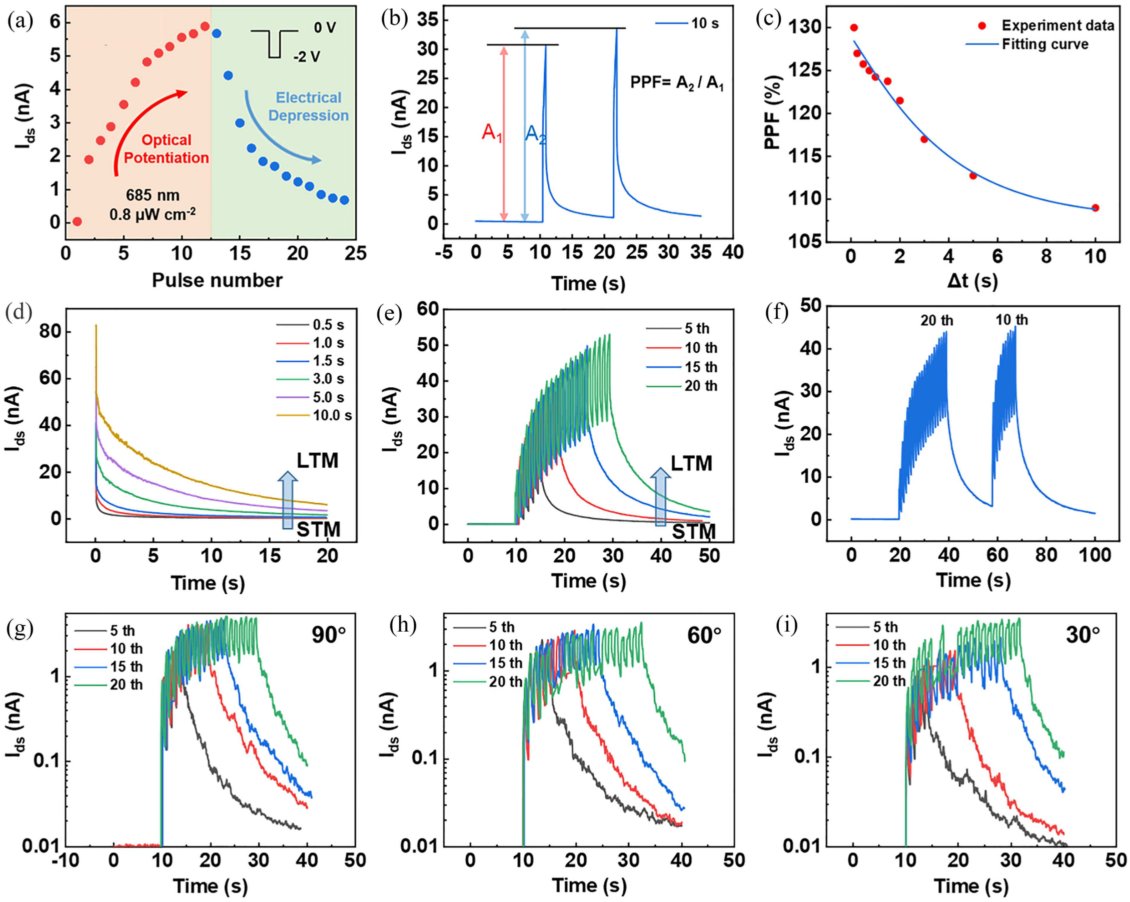

Figure 3 (Color online) Biomimetic simulation of MoS_2 synaptic transistor manufactured by one-step method. (a) Impulse response test. (b) Double pulse facilitation (PPF = A_2/A_1). (c) PPF size depends on the time interval Δt between the double pulses. (d) Different pulse widths dominated EPSC of the device with the same pulse numbers. (e) Different pulse number dominated EPSC of the device with the same pulse widths. (f) Learning-forget-relearning simulation process. The EPSC changes of the device when stimulated by different numbers of pulses at (g) 90°, (h) 60°, and (i) 30°.

defined as written. Subsequently, after the device is electrically erased by 12 gate voltage pulses, the PSC of the device gradually decreases to the initial value. This decrease can be attributed to the acceleration of carrier recombination induced by the gate voltage.

Double pulse facilitation (PPF) is a significant biological phenomenon wherein a synapse is subjected to two identical external stimuli in a short period, resulting in a response current produced by the second stimulus that is higher than that of the first. The ratio of the second current to the first current is related to the time interval between the two stimuli [46–48]. Figure 3(b) illustrates PPF stimulated by two continuous light pulses with a pulse interval of 10 s. PPF tests at different pulse intervals are depicted in Figure S7, demonstrating that the PSC generated by the second pulse stimulation exceeds the response current generated by the first pulse stimulation. This observation indicates the successful simulation of PPF behavior. Additionally, the PPF index serves as an important parameter to evaluate the performance of the synaptic device and can be described by the following formula:

$$\mathrm{PPF} = \frac{A_2}{A_1} \times 100\%, \tag{1}$$

where A_2 and A_1 represent EPSC values generated by the second input pulse signal and the first input pulse signal respectively. The change of the PPF index of the MoS_2 synaptic transistor with the time interval is shown in Figure 3(c). Its magnitude decreases with the increase of the time interval, and then gradually approaches the constant 1. This is because when the Δt is large enough, the electron-hole pairs in the channel have enough time to recombine and return the device to its equilibrium state. When PPF = 1, it means that the maximum current value achieved by the two light pulse stimuli is the same, which represents that the effect of the first stimulus has been completely forgotten. The attenuation trajectory of the PPF index can be described using a double exponential function, as follows [49]:

$$\mathrm{PPF} = 1 + C_1 \times \exp\left(-\frac{t}{\tau_1}\right) + C_2 \times \exp\left(-\frac{t}{\tau_2}\right), \tag{2}$$

where t represents the time interval, C_1 and C_2 are the coefficient factors, and τ_1 and τ_2 are the characteristic relaxation time. Figure 3(c) shows that the PPF attenuation behavior of MoS_2 synaptic transistor is consistent with this equation. The data fitting results show that the values of τ_1 and τ_2 are 1.21 and 3.31 respectively, and τ_1 is smaller than τ_2, which accords with the response time of biological synapses.

Short-term memory (STM) and long-term memory (LTM) typically refer to distinct types of memory, with the primary difference lying in memory duration [50, 51]. STM typically lasts for hundreds or thousands of milliseconds, whereas LTM refers to a longer-lasting memory consolidation process. The transition from STM to LTM often occurs through repeated rehearsal and training processes, where memory strength depends on the intensity and frequency of learning [52]. MoS_2 synaptic transistors can be utilized to simulate this transition process, treating input light pulse stimulation as the training process and the resulting PSC as the memory effect. Figure 3(d) depicts the EPSC changes of the device at different pulse widths (685 nm, 1.4 $\mu W \cdot cm^{-2}$). It is observed that EPSC gradually increases with the duration of the pulse, and the decay time becomes longer. This process mirrors the phenomenon observed in the human brain after prolonged training, where synaptic weights increase, leading to the formation of long-term memory. The SRDP behavior of the synapse is demonstrated in Figure 3(e), showing a similar phenomenon in EPSCs with different pulse number devices, indicating that the transition from STM to LTM was successfully simulated by increasing pulse width and number. The device manufactured in the repeatability verification can also realize the behavior transformation of PPF and STM to LTM, as shown in Figure S8.

In biology, the brain acquires new knowledge through a three-step process: learning, forgetting, and relearning. It is often easier to recall previously learned information during relearning than during the initial learning process. Figure 3(f) illustrates the learning, forgetting, and relearning process of the MoS_2 synaptic transistor. In this process, the attenuation of the current after 20 light pulse inputs represents the forgetting process. Remarkably, only 10 consecutive light pulses are needed to restore the MoS_2 synaptic transistor to the storage level during the relearning process, which is half the number of light pulses required during the initial learning process. This behavior closely mirrors the learning and memory processes observed in the human brain.

In the nervous system, in addition to one-to-one axon-dendrite synapses, there are also multi-to-one axon-cellular synapses. The synaptic nerve cell body typically receives synaptic input from multiple other nerve axons originating from different directions. To simulate this phenomenon, we investigated the synaptic plasticity of MoS_2 synaptic transistors at 90°, 60° and 30° with different pulse numbers of lasers in the visible light band, as shown in Figures 3(g)–(i). In addition, we also carried out the continuous change of the current of the device under the condition that the incident angle of the device gradually becomes 0° from 90°, as shown in Figure S9. The results indicate that under the three incident angles, the device can exhibit transition behavior from STM to LTM with an increase in pulse number. This suggests that the MoS_2 synaptic transistor maintains good synaptic plasticity even at small incident angle, which enable the imitation of the multi-to-one axon-cellular synapses by this proposed device.

Pavlov's dog conditioning is the cognitive behavior of neural networks and it is a classical application to demonstrate the performance of synaptic device (Figure 4(a)). Accordingly, Pavlov's dog conditioning is simulated by employing a gate voltage (+10 V) as a food (unconditioned) stimulus and a light pulse (685 nm, 1.4 $\mu W \cdot cm^{-2}$) as a ringtone (conditioned) stimulus with the proposed one-step manufactured MoS_2 synaptic transistor. The pulse width and pulse interval are both set to 1000 ms. Before the training period, 20 light stimuli are applied to the device and the synaptic weight remained below the threshold value (65 nA), indicating the non-activation of salivation, as depicted in Figure 4(b). During the training process, when a gate voltage of +10 V was applied to the device concurrently with 20 light stimuli, the synaptic weight increased to 75 nA. At this point, the current surpassed the threshold current, signifying the activation of salivation under food stimulation. Following the training, when only 20 light stimuli were administered, the synaptic weight remained higher than the threshold, indicating the establishment of an association between the food and the bell (Figure 4(c)).

Finally, to simulate image processing in the brain, a 3 × 3 synaptic transistor array is constructed to achieve multi-view image feature extraction, as depicted in Figure S10. The width and interval of the light pulses (685 nm, 1.15 $\mu W \cdot cm^{-2}$) used are 1 s. The pixels in the array were labeled as pixel 1 to

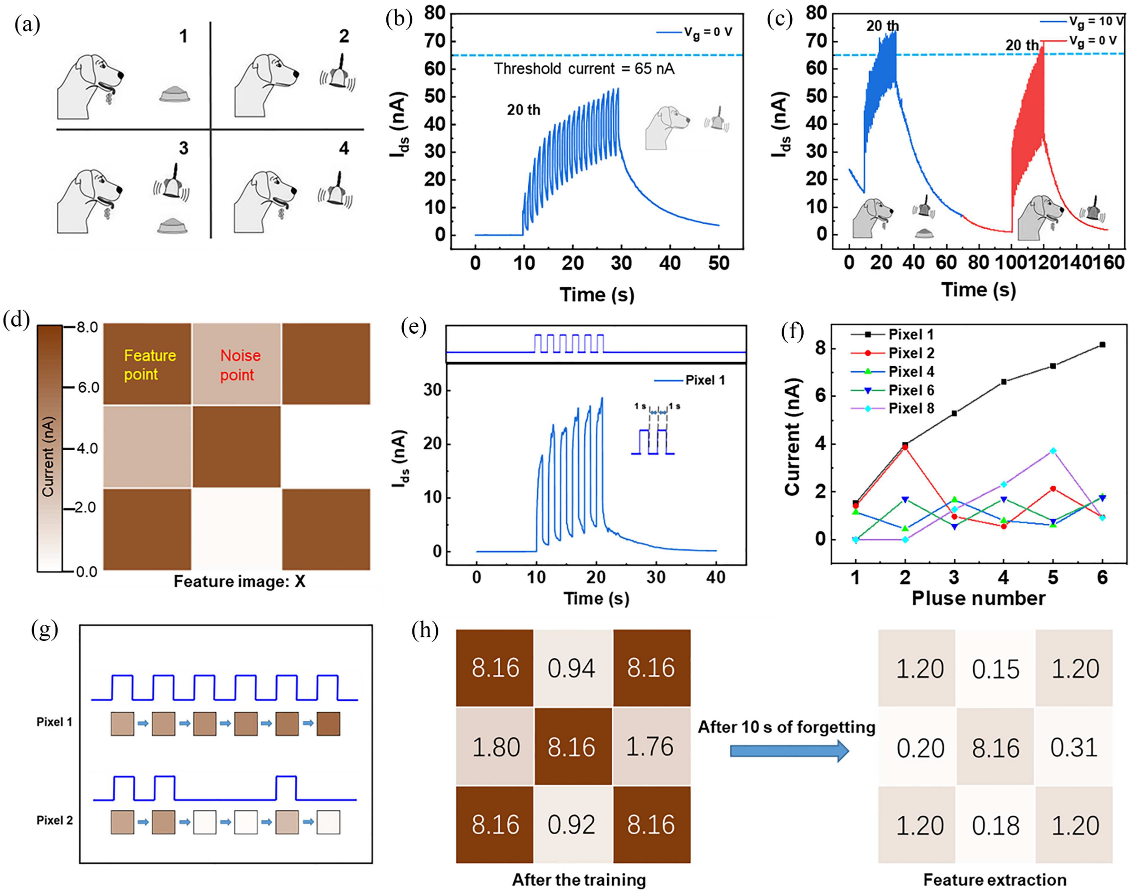

Figure 4 (Color online) Conditioned reflex simulation and multi-view feature extraction. (a) Schematic diagram of the experiment of a classic Pavlov dog; (b) before training; (c) during and after training; (d) the relationship between the current value and gray value, the feature image is "X"; (e) the current change of pixel 1 under pulse stimulation; (f) current change of each pixel under pulse stimulation; (g) the change of the grayscale image of pixel 1 and pixel 2 with pulse stimulation; (h) image feature extraction.

pixel 9, and the stimulation of the image to the pixels in the array varied. Specifically, the five pixels corresponding to the feature image "X" received the same pulse stimulation, while pixels 2, 4, 6, and 8 received completely different pulse stimulation. Figure 4(d) shows the relationship between the current value and the gray value, and the feature image is "X". Additionally, Figure S11 displays six images with noise, each sharing the common feature "X" and containing two noise points unique to that image. When the six images are illuminated on the array in turn, pixel 1 will be stimulated by six consecutive light pulses, as shown in Figure 4(e). The current after each stimulus increased compared to the previous one, indicating continuous learning. Conversely, the light pulse stimulation of pixels 2, 4, 6, and 8 in the non-feature image positions was discontinuous, as depicted in Figure S12. The increase in these currents was minimal due to the learning and forgetting process, resulting in a progressively larger difference between the currents of the two types of pixels (Figure 4(f)). When the current values were converted to gray values, the increasing difference in current represented a noticeable color difference. As depicted in Figure 4(g), the image color of pixel 1 continues to deepen, while the image color of pixel 2 does not change in the same way. Figure 4(h) illustrates the feature extraction of the images. After training, a significant contrast between the feature points and noise points was observed. After 10 s of forgetting, the common feature "X" across the six images was ultimately obtained. Thus, adjusting the frequency of light can enhance the contrast of grayscale images, holding promising prospects for analog neuromorphic vision systems.

3 Experiment methods

Device fabrication. First, the n^+ Si/SiO_2 substrate is cleaned with acetone, ethanol, and deionized water. Subsequently, two-dimensional MoS_2 was deposited on the substrate using the mechanical exfoliation and dry transfer method. Then, two different approaches are integrated to fabricate the electrodes. The first one involves the utilization of ultraviolet lithography (MicroTec SUSS MJB4) and magnetron sputtering (Discovery 635) to fabricate the source and drain electrodes (Au 70 nm) on the MoS_2 surface. The second approach involves the use of ultraviolet lithography and metal film transferred method, wherein the thickness of the transferred source and drain electrodes is also 70 nm.

Device characterization. The optical images of the MoS_2 FET were obtained using an optical microscope. The thickness of molybdenum disulfide was determined using the Atomic Force Microscope (Bruker multimode 8). The Raman spectra of molybdenum disulfide were obtained using the Raman technique (WITec alpha300). An LED laser light source and a waveform generator are used to produce light pulse stimulation. A semiconductor device analyzer (B1500A) is used to collect the electrical measurements of all devices.

4 Conclusion

In summary, we propose a one-step manufactured MoS_2 synaptic transistor, which combines the metal electrode deposition with the introduction of defect states to simplify the preparation process and structure of the synaptic FET. Through experimental validation, we have confirmed the feasibility of the proposed approach. We conducted comprehensive studies on the synaptic plasticity of the one-step MoS_2 synaptic transistor. Our device exhibits both the LTP and LTD under photoelectric coordination. Furthermore, we thoroughly investigated the biological simulation of the device, which helped achieve the transformation of PPF and short-term memory to long-term memory. It is worth noting that our artificial synapses emulate functions akin to human learning, forgetting, and relearning. Moreover, the fabricated devices exhibit robust synaptic plasticity across various incident light angles, demonstrating the capability of a multi-to-one axon-cellular synapse imitation. Finally, we successfully simulate the classic Pavlovian dog conditioned reflex, and we demonstrate the functionality of multiview feature extraction in image processing. The results indicate a great potential of the proposed one-step manufacture MoS_2 synaptic FET for future huge-scale bionic integration with standard and simple integrated circuits manufacture technology.

Acknowledgements This work was supported by National Natural Science Foundation of China (Grant Nos. 62305013, 62334001, U23A20357) and China National Postdoctoral Program for Innovative Talents (Grant No. BX20230033).

Supporting information Figures S1–S12. The supporting information is available online at info.scichina.com and link.springer.com. The supporting materials are published as submitted, without typesetting or editing. The responsibility for scientific accuracy and content remains entirely with the authors.

References

1 Fuller E J, Keene S T, Melianas A, et al. Parallel programming of an ionic floating-gate memory array for scalable neuromorphic computing. Science, 2019, 364: 570–574
2 Xia Q, Yang J J. Memristive crossbar arrays for brain-inspired computing. Nat Mater, 2019, 18: 309–323
3 Zidan M A, Strachan J P, Lu W D. The future of electronics based on memristive systems. Nat Electron, 2018, 1: 22–29
4 Sun J, Oh S, Choi Y, et al. Optoelectronic synapse based on IGZO-alkylated graphene oxide hybrid structure. Adv Funct Mater, 2018, 28: 1804397
5 Han P, Hanlon D, Arshad N, et al. Platelet P-selectin initiates cross-presentation and dendritic cell differentiation in blood monocytes. Sci Adv, 2020, 6: eaaz1580
6 Li R, Peng B. Implementing monocular visual-tactile sensors for robust manipulation. Cyborg Bionic Syst, 2022, 2022: 9797562
7 Ahmed T, Kuriakose S, Mayes E L H, et al. Optically stimulated artificial synapse based on layered black phosphorus. Small, 2019, 15: 1900966
8 Han S, Ma T, Li H, et al. Photoferroelectric perovskite synapses for neuromorphic computing. Adv Funct Mater, 2023, 34: 2309910
9 Sun Y, Li M, Ding Y, et al. Programmable van-der-Waals heterostructure-enabled optoelectronic synaptic floating-gate transistors with ultra-low energy consumption. InfoMat, 2022, 4: e12317
10 Yang H, Hu Y, Zhang X, et al. Near-infrared optical synapses based on multilayer $MoSe_2$ Moiré superlattice for artificial retina. Adv Funct Mater, 2023, 34: 2308149
11 Boybat I, Le Gallo M, Nandakumar S R, et al. Neuromorphic computing with multi-memristive synapses. Nat Commun, 2018, 9: 2514
12 Wu Y, Deng W J, Chen X Q, et al. CMOS-compatible retinomorphic Si photodetector for motion detection. Sci China Inf Sci, 2023, 66: 162401
13 Li Y Y, Wang Y, Yin L, et al. Silicon-based inorganic-organic hybrid optoelectronic synaptic devices simulating cross-modal learning. Sci China Inf Sci, 2021, 64: 162401
14 Hao D D, Yang D, Liang H X, et al. Lead-free perovskites-based photonic synaptic devices with zero electric energy consumption. Sci China Inf Sci, 2024, 67: 162401
15 Ielmini D, Wong H S P. In-memory computing with resistive switching devices. Nat Electron, 2018, 1: 333–343
16 Wang T, Meng J, Chen L, et al. Flexible 3D memristor array for binary storage and multi-states neuromorphic computing applications. InfoMat, 2020, 3: 212–221

17 Zhang M, Fan Z, Jiang X, et al. MoS_2-based charge-trapping synaptic device with electrical and optical modulated conductance. Nanophotonics, 2020, 9: 2475–2486
18 Zhang C, Ning J, Wang B, et al. A dual-mode programing nonvolatile floating-gate memory with convertible Ohmic and Schottky contacts. Adv Elect Mater, 2024, 10: 2300503
19 Du J, Ge C, Riahi H, et al. Dual-gated MoS_2 transistors for synaptic and programmable logic functions. Adv Elect Mater, 2020, 6: 1901408
20 Huh W, Lee D, Jang S, et al. Heterosynaptic MoS_2 memtransistors emulating biological neuromodulation for energy-efficient neuromorphic electronics. Adv Mater, 2023, 35: 2211525
21 Wang X, Wang B, Zhang Q, et al. Grain-boundary engineering of monolayer MoS_2 for energy-efficient lateral synaptic devices. Adv Mater, 2021, 33: 2102435
22 Yu J, Kim Y, Lee C, et al. Bio-inspired organic synaptor with in situ ion-doped ultrathin polyelectrolyte containing acetylcholine-like cation. Small, 2024, 20: 2312283
23 Cho H, Lee D, Ko K, et al. Double-floating-gate van der Waals transistor for high-precision synaptic operations. ACS Nano, 2023, 17: 7384–7393
24 Zhao T, Zhao C, Xu W, et al. Bio-inspired photoelectric artificial synapse based on two-dimensional $Ti_3C_2T_x$ MXenes floating gate. Adv Funct Mater, 2021, 31: 2106000
25 Liu K, Zhang T, Dang B, et al. An optoelectronic synapse based on α-In_2Se_3 with controllable temporal dynamics for multimode and multiscale reservoir computing. Nat Electron, 2022, 5: 761–773
26 Kwon K C, Zhang Y, Wang L, et al. In-plane ferroelectric tin monosulfide and its application in a ferroelectric analog synaptic device. ACS Nano, 2020, 14: 7628–7638
27 Lin S, Zhang G, Lai Q, et al. Recent advances in layered two-dimensional ferroelectrics from material to device. Adv Funct Mater, 2023, 33: 2304139
28 Hong C, Oh S, Dat V K, et al. Engineering electrode interfaces for telecom-band photodetection in MoS_2/Au heterostructures via sub-band light absorption. Light Sci Appl, 2023, 12: 280
29 Liu L, Kong L, Li Q, et al. Transferred van der Waals metal electrodes for sub-1-nm MoS_2 vertical transistors. Nat Electron, 2021, 4: 342–347
30 Liu Y, Guo J, Zhu E, et al. Approaching the Schottky-Mott limit in van der Waals metal-semiconductor junctions. Nature, 2018, 557: 696–700
31 Zheng W, Saiz F, Shen Y, et al. Defect-free metal deposition on 2D materials via inkjet printing technology. Adv Mater, 2021, 34: 2104138
32 Vandalon V, Sharma A, Perrotta A, et al. Polarized Raman spectroscopy to elucidate the texture of synthesized MoS_2. Nanoscale, 2019, 11: 22860–22870
33 Verble J L, Wieting T J. Lattice mode degeneracy in MoS_2 and other layer compounds. Phys Rev Lett, 1970, 25: 362–365
34 Zhang X, Han W P, Wu J B, et al. Raman spectroscopy of shear and layer breathing modes in multilayer MoS_2. Phys Rev B, 2013, 87: 115413
35 Zhang X, Tan Q H, Wu J B, et al. Review on the Raman spectroscopy of different types of layered materials. Nanoscale, 2016, 8: 6435–6450
36 Bae S, Sugiyama N, Matsuo T, et al. Defect-induced vibration modes of Ar^+-irradiated MoS_2. Phys Rev Appl, 2017, 7: 024001
37 Mignuzzi S, Pollard A J, Bonini N, et al. Effect of disorder on Raman scattering of single-layer MoS_2. Phys Rev B, 2015, 91: 195411
38 Kou Z, Hashemi A, Puska M J, et al. Simulating Raman spectra by combining first-principles and empirical potential approaches with application to defective MoS_2. npj Comput Mater, 2020, 6: 59
39 Huang B, Tian F, Shen Y, et al. Selective engineering of chalcogen defects in MoS_2 by low-energy helium plasma. ACS Appl Mater Interfaces, 2019, 11: 24404–24411
40 Kang N, Paudel H P, Leuenberger M N, et al. Photoluminescence quenching in single-layer MoS_2 via oxygen plasma treatment. J Phys Chem C, 2014, 118: 21258–21263
41 Grünleitner T, Henning A, Bissolo M, et al. Real-time investigation of sulfur vacancy generation and passivation in monolayer molybdenum disulfide via in situ X-ray photoelectron spectromicroscopy. ACS Nano, 2022, 16: 20364–20375
42 Komsa H P, Krasheninnikov A V. Native defects in bulk and monolayer MoS_2 from first principles. Phys Rev B, 2015, 91: 125304
43 Noh J Y, Kim H, Kim Y S. Stability and electronic structures of native defects in single-layer MoS_2. Phys Rev B, 2014, 89: 205417
44 Zhang X, Wang S, Lee C K, et al. Unravelling the effect of sulfur vacancies on the electronic structure of the MoS_2 crystal. Phys Chem Chem Phys, 2020, 22: 21776–21783
45 Li M, Xiong Z, Shao S, et al. Multimodal optoelectronic neuromorphic electronics based on lead-free perovskite-mixed carbon nanotubes. Carbon, 2021, 176: 592–601
46 Jiang J, Guo J, Wan X, et al. 2D MoS_2 neuromorphic devices for brain-like computational systems. Small, 2017, 13: 1700933
47 Hu W, Jiang J, Xie D, et al. Proton-electron-coupled MoS_2 synaptic transistors with a natural renewable biopolymer neurotransmitter for brain-inspired neuromorphic learning. J Mater Chem C, 2019, 7: 682–691
48 Wang L, Wei S, Xie J, et al. Artificial synapses based on an optical/electrical biomemristor. Nanomaterials, 2023, 13: 3012
49 Choi Y, Kim J H, Qian C, et al. Gate-tunable synaptic dynamics of ferroelectric-coupled carbon-nanotube transistors. ACS Appl Mater Interfaces, 2020, 12: 4707–4714
50 Coltheart M. Iconic memory. Philos Trans R Soc Lond B Biol Sci, 1983, 302: 283–294
51 Haber R N. The impending demise of the icon: a critique of the concept of iconic storage in visual information processing. Behav Brain Sci, 1983, 6: 1–11
52 Hua Z, Yang B, Zhang J, et al. Monolayer molecular crystals for low-energy consumption optical synaptic transistors. Nano Res, 2022, 15: 7639–7645